OPEN

Citation: Cell Death and Disease (2014) 5, e1328; doi:10.1038/cddis.2014.288
© 2014 Macmillan Publishers Limited All rights reserved 2041-4889/14
www.nature.com/cddis

Autophagy and mitochondrial alterations in human retinal pigment epithelial cells induced by ethanol: implications of 4-hydroxy-nonenal

M Flores-Bellver[1,5], L Bonet-Ponce[1,5], JM Barcia[1], JM Garcia-Verdugo[2], N Martinez-Gil[1], S Saez-Atienzar[1], J Sancho-Pelluz[1], J Jordan[3], MF Galindo[4] and FJ Romero*[,1]

Retinal pigment epithelium has a crucial role in the physiology and pathophysiology of the retina due to its location and metabolism. Oxidative damage has been demonstrated as a pathogenic mechanism in several retinal diseases, and reactive oxygen species are certainly important by-products of ethanol (EtOH) metabolism. Autophagy has been shown to exert a protective effect in different cellular and animal models. Thus, in our model, EtOH treatment increases autophagy flux, in a concentration-dependent manner. Mitochondrial morphology seems to be clearly altered under EtOH exposure, leading to an apparent increase in mitochondrial fission. An increase in 2′,7′-dichlorofluorescein fluorescence and accumulation of lipid peroxidation products, such as 4-hydroxy-nonenal (4-HNE), among others were confirmed. The characterization of these structures confirmed their nature as aggresomes. Hence, autophagy seems to have a cytoprotective role in ARPE-19 cells under EtOH damage, by degrading fragmented mitochondria and 4-HNE aggresomes. Herein, we describe the central implication of autophagy in human retinal pigment epithelial cells upon oxidative stress induced by EtOH, with possible implications for other conditions and diseases.
Cell Death and Disease (2014) **5,** e1328; doi:10.1038/cddis.2014.288; published online 17 July 2014

Retinal pigment epithelium (RPE) is a single neuroectodermal layer placed in the outermost part of the eye cup faced to photoreceptors.[1,2] Owing to its anatomical location and function, RPE is continuously exposed to potential cell damage caused by oxidative stress, specifically due to oxygen and nitrogen reactive species.[3] This is probably one of the reasons why these cells are more resistant to oxidative stress.[4] Oxidative stress is present as part of the pathophysiology in several retinal degenerations associated with blindness, for example, age-related macular degeneration,[3] where RPE is considered a key factor for its development.[5] Studies with the human-derived cell line ARPE-19 have proven to be very useful in the elucidation of the role of these cells in disease.

Autophagy is a catabolic process aimed to degrade damaged organelles, proteins and cellular debris by engulfing them into a double membrane vesicle called the autophagosome and eliminating them by posterior fusion with the lysosome. Activation of macroautophagy, a form of autophagy, has been recently confirmed to be a primary response of ARPE-19 cells to stress.[6] Furthermore, the two major functions of RPE, phagocytosis of the photoreceptor outer segments and visual cycle performance, have been linked to a noncanonical form of autophagy that is known as LC3 (microtubule-associated protein 1A/1B-light chain 3)-associated phagocytosis and is supposed to contribute to the normal supply of vitamin A and therefore to normal vision.[7,8]

Despite its negative effects on health, ethanol (EtOH) is consumed daily worldwide, standing as one of the top public health challenges. EtOH induces morphological and physiological changes in the nervous tissue, and most of these changes may be attributed to reactive oxygen species (ROS), as they can be normalized or prevented by antioxidant treatments.[9–13] Autophagy has been identified as cytoprotector in nervous and liver cells under EtOH-induced toxicity,[14,15] where it seems to degrade damaged organelles, including mitochondria. Recent findings support the idea that there is an increased mitochondrial stress and dysfunction in the RPE cells in AMD patients.[16,17] Oxidative-damaged

[1]Department of Physiology, School of Medicine and Dentistry, Catholic University of Valencia, Valencia, Spain; [2]Department of Comparative Neurobiology, Cavanilles Institute of Biodiversity and Evolutive Biology, University of Valencia, Valencia, Spain; [3]Neuropharmacology Group, Department of Medical Sciences, School of Medicine, University of Castilla la Mancha, IDINE, Albacete, Spain and [4]Unit of Translational Neuropsychopharmacology, University of Castilla la Mancha and Albacete Hospital, Albacete, Spain

*Corresponding author: FJ Romero, Facultad de Medicina y Odontología, Universidad Católica de Valencia 'San Vicente Martir', Calle Quevedo 2, Valencia 46010, Spain. Tel: +34 96 363 74 12; Fax: +34 96 394 45 90; E-mail: fj.romero@ucv.es

[5]These authors contributed equally to this work.

Abbreviations: RPE, retinal pigment epithelium; LC3, microtubule-associated protein 1A/1B-light chain 3; EtOH, etanol; ROS, reactive oxygen species; PD, Parkinson's disease; AD, Alzheimer's disease; HD, Huntington's disease; HAE, hydroxyalkenals; 4-HNE, 4-hydroxy-2,3-trans-nonenal; V-FITC, V-fluorescein isothiocyanate; PI, propidium iodide; TUNEL, terminal deoxynucleotidyl transferase dUTP nick end labeling; ER, endoplasmic reticulum; ERAD, associated degradation; PE, phosphatidylethanolamine; CQ, cloroquine; GFP, green fluorescent protein; RFP, red fluorescent protein; 3-MA, 3-methyl-adenine; DCFH, 2',7'-dichlorofluorescein; MDA, malondialdehyde; HDAC6, histone deacetylase 6; DCF, dichlorofluorescein; GADPH, glyceraldehyde 3-phosphate dehydrogenase; IgG, immunoglobulin G; ECL, enhanced chemiluminescence; DAPI, 4,6-diamidino-2-phenylindole; LSM, laser scanning microscope

Received 21.3.14; revised 05.6.14; accepted 06.6.14; Edited by GM Fimia

mitochondria, a main source of ROS, seem to be removed by autophagy (known as mitophagy), in order to guarantee cell survival.[18] As a matter of fact, deregulation of mitophagy has been implicated in several neurodegenerative diseases, such as Parkinson's disease (PD), Alzheimer's disease (AD) and Huntington's disease (HD).

Peroxidation of polyunsaturated fatty acids is intensified in cells subjected to oxidative stress, and results in the generation of various bioactive compounds, among others 4-hydroxyalkenals (HAE). ROS-induced lipid peroxidation and the resulting HAE markedly contribute to the development and progression of different diseases.[19] Specifically, 4-hydroxy-nonenal (4-HNE), a major α,β-unsaturated aldehyde product of n-6 fatty acid oxidation, has been shown to be involved in a great number of maladies.[20] It has been reported that 4-HNE induces apoptosis in ARPE-19 cells[21] and its ability to form protein adducts, thus it seems to be a key factor in aggresome formation. Aggresome is a term referred to cytoplasmic perinuclear inclusion bodies formed by aggregated proteins.[22] Indeed, the presence of aggresomes is a pathological hallmark of most neurodegenerative diseases, and 4-HNE seems to be involved in their formation in AD,[23] PD,[24] HD[25] and amyotrophic lateral sclerosis.[26] These aggresomes depend on the protein type to be cleared,[27,28] and their degradation by autophagy, known as aggrephagy, has been proposed to increase cell viability in neurodegeneration models.[29] Interestingly, 4-HNE aggregates have been also found in hepatic cells from alcoholic patients.[30–32] Recent data provide no clear cut evidence of a link between PD risk and alcohol consumption with both positive[33] and negative[34] results.

In this study, we report the cellular effects of EtOH on ARPE-19 cells and determine that EtOH exposure induces the formation of 4-HNE-aggresomes, together with other neurodegenerative hallmarks such as mitochondrial damage and autophagy activation. Considering the central role of RPE in retinal physiology and pathophysiology, and its neural origin, these findings render new insights into the mechanism of neurodegeneration caused by alcohol toxicity in retinal cells, and may contribute to the development of therapeutic strategies in several nervous and retinal diseases.

Results

EtOH induces toxicity in ARPE-19 cells. EtOH treatment produced a statistically significant reduction of mitochondrial

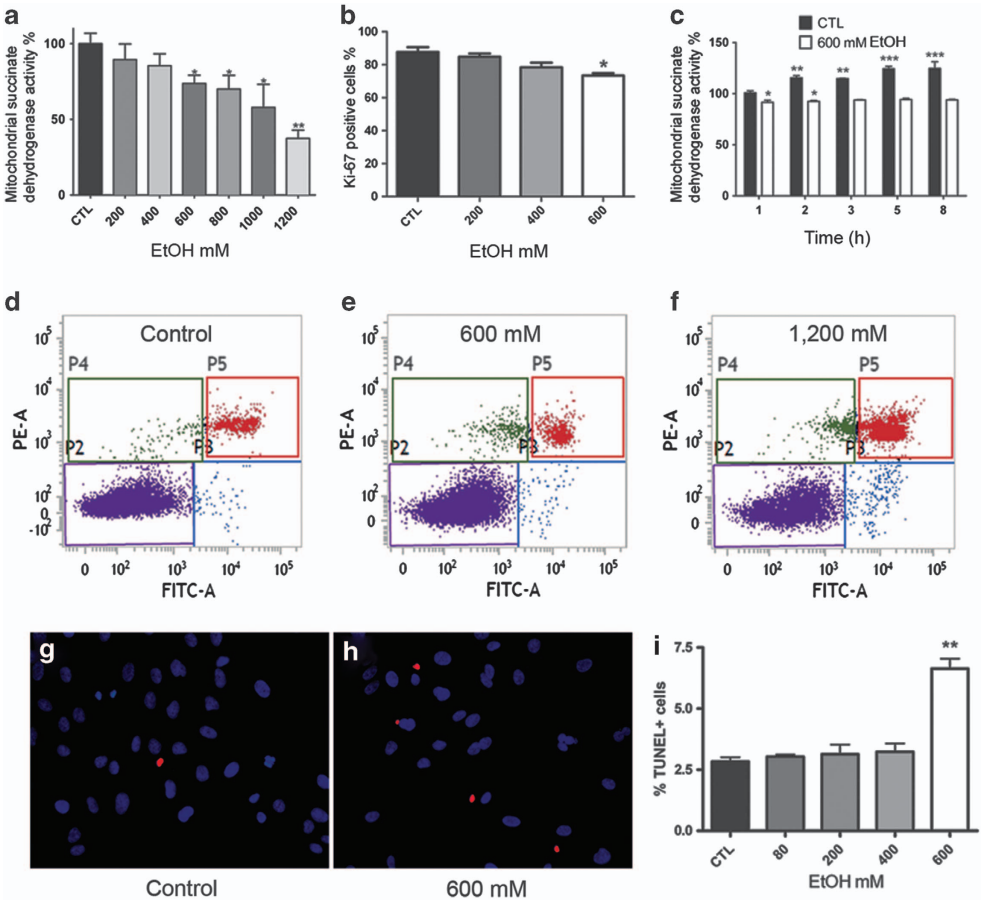

Figure 1 Proliferation and cell death of EtOH-treated and non-treated ARPE-19 cells. MTT assay after 24 h of EtOH exposure at different concentrations (**a**). Ki-67 immunocytochemistry analysis (**b**). MTT assay along the first 8 h after 600 mM EtOH exposure (**c**). Flow cytometry measures of V-FITC and PI (PE-A) of control (**d**), 600 mM (**e**) and 1200 mM (**f**) EtOH in ARPE-19 cells. TUNEL analysis of control (**g**) and 600 mM EtOH (**h**), cell nuclei stained with DAPI (blue) and TUNEL-positive cells (red). Graphic representation of the percentage of TUNEL-positive cells after EtOH treatment (**i**). Values are expressed as mean ± S.E.M. ($N = 4$). Statistical significance was determined by one-way ANOVA test and Bonferroni analysis (*$P < 0.05$, **$P < 0.01$ and ***$P < 0.001$)

activity in a concentration-dependent manner after 24 h of exposure, starting at 600 mM (Figure 1a). Ki-67 immunocytochemistry showed a reduction of the number of positive cells, suggesting cell cycle suppression (Figure 1b). Interestingly, a statistically significant reduction of MTT-positive cells occurred in the first 60 min of treatment, and a more gradual decrease was observed during the following 8 h after the addition of 600 mM EtOH (Figure 1c). Annexin V-fluoroscein isothiocyanate (V-FITC) and propidium iodide (PI) staining were analyzed by flow cytometry, demonstrating a tendency but no statistically significant differences in cell death at this concentration of EtOH (Figures 1d and e). As a positive control, we confirmed that EtOH produced a significant increase in cell death at 1200 mM (Figure 1f) as previously described.[35] The terminal deoxynucleotidyl transferase dUTP nick end labeling (TUNEL) assay was also performed and significant changes were observed between control (Figure 1g) and treated cells only at 600 mM EtOH concentration (Figures 1h and i). Although such small change seems unimportant, it marks the beginning of a cascade, which may threat the destiny of the cell.

As Bcl-2 and Bax are both mitochondrial membrane-related proteins, respectively, implicated in protection and apoptosis, we analyzed Bcl-2, Bax and uncleaved caspase-3 expression levels in order to foresee cellular fate in our experimental conditions. Bcl-2 and Bax expression levels were significantly enhanced 24 h after the addition of 600 mM EtOH, when compared with the control group (Figures 2a–c). Interestingly, a statistically significant increase of uncleaved caspase-3 expression was found at 600 mM EtOH treatment (Figure 2d).

EtOH exposure induces autophagy. LC3 is used as a specific marker of autophagosomes. LC3 exists in two different forms within the cell: LC3-I, which is distributed in the cytoplasm and LC3-II, which is converted from LC3-I and is covalently bound to the membrane lipid phosphatidylethanolamine in the autophagosomal membranes. LC3-II is therefore crucial to initiate the autophagosome formation. LC3-I function in the cell is autophagy independent. Indeed, LC3-I has been proposed to have a role in the vesicle-mediated removal of endoplasmic reticulum (ER)-associated degradation (ERAD) regulators.[36,37] Defectively folded proteins in the ER are selectively degraded by a group of proteins called ERAD. An increase of ERAD activity could lead to a degradation of correctively folded proteins, thus a correct regulation of ERAD is crucial to maintain cellular

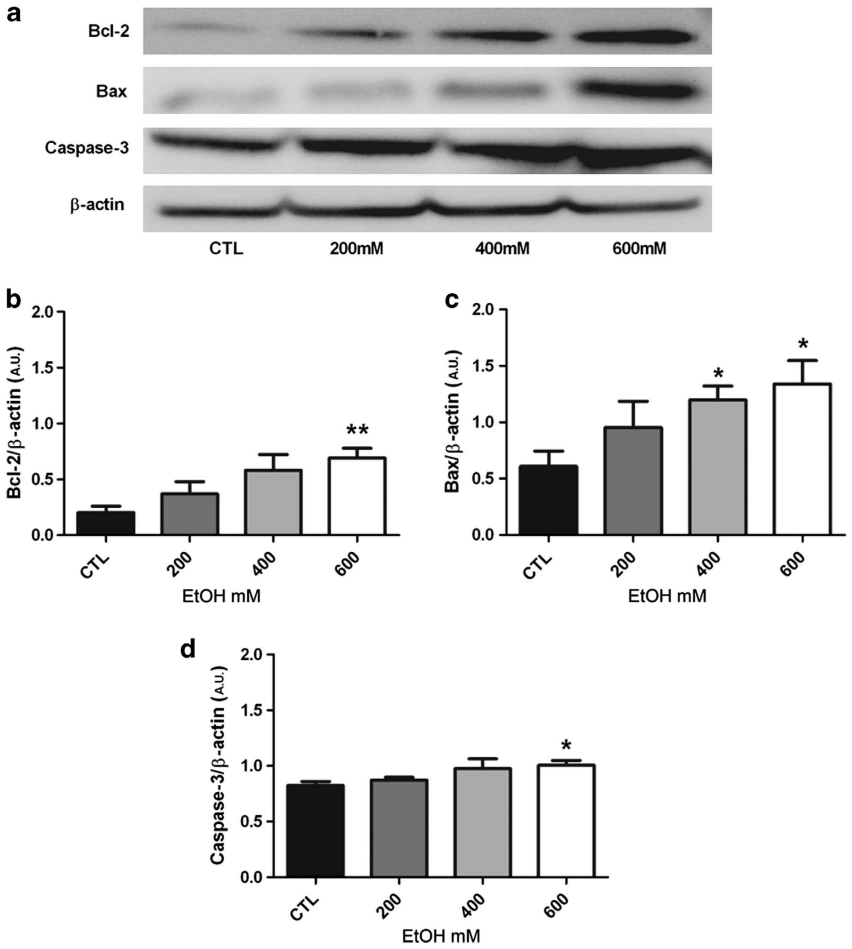

Figure 2 Pro-survival and pro-apoptotic mitochondrial protein expression. Protein expression analyzed by western blot of Bcl-2, Bax, uncleaved caspase-3 and α-actin in control and EtOH-treated ARPE-19 cells (**a**). Graphic representations of semiquantitative analysis of Bcl-2 (**b**), Bax (**c**) and uncleaved caspase-3 (**d**). Values are expressed as mean ± S.E.M. ($N = 3$). Statistical significance was determined by two-tailed Student's *t*-test (*$P < 0.05$ and **$P < 0.01$)

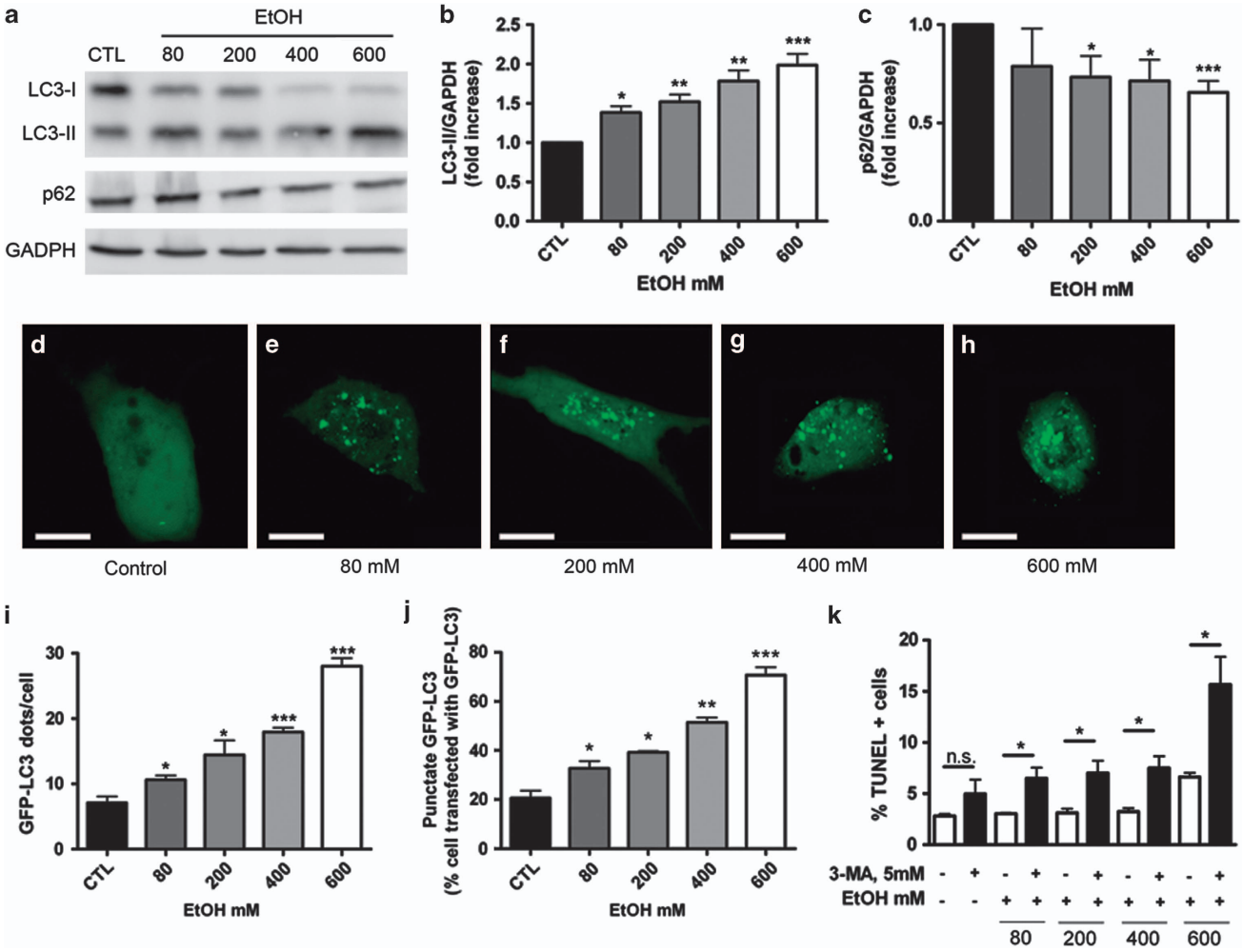

Figure 3 EtOH treatment increases autophagosome number in ARPE-19 cells. Protein expression analyzed by western blot of LC3-II, p62 and GAPDH (**a**). Graphic representation of semiquantitative analysis of LC3-II (**b**) and p62 (**c**). Cells were transfected with GFP-LC3 plasmid. Expression of GFP-LC3 dots were observed in control cells (**d**) and treated at 80 mM (**e**), 200 mM (**f**), 400 mM (**g**) and 600 mM EtOH (**h**). Quantification of GFP-LC3 dots per cell (**i**) and autophagic cells at different EtOH concentrations (**j**). Representative analysis of cell death (percentage of TUNEL-positive cells) challenged or not with 80, 200, 400 and 600 mM of EtOH and 3-MA (**k**). Values are expressed as mean ± S.E.M. ($N=3$). Statistical significance was determined by a two-tailed Student's *t*-test (*$P<0.05$, **$P<0.01$ and ***$P<0.001$). Scale bars: 12 μm

homeostasis. At steady-state, ERAD regulators are removed from the ER through a vesicle-mediated mechanism. LC3-I, therefore, has a role as a membrane-bound receptor that ensures the vesicle-mediated removal of ERAD regulators. Thus, GFP-LC3 overexpression is a well-accepted assessment of autophagosome formation. Small amounts of GFP-LC3 dots were observed (<9 dots) in control cells (Figure 3d). Conversely, the addition of 80, 200, 400 or 600 mM EtOH significantly increased the number of GFP-LC3 dots per cell and the percentage of autophagic cells (cells with >9 dots per cell) in a concentration-dependent manner (Figures 3e–j). Immunoblot analysis confirmed the increase of the membrane-associated PE-conjugated LC3 (LC3-II) in EtOH-treated cells, in a concentration-dependent manner (Figures 3a and b).

Accumulation of autophagosomes may be due to an increase of autophagosome synthesis, disruption of autophagosome–lysosome fusion or both. We used the lysosome inhibitor chloroquine (CQ), which clamps the degradation, to study the effect of EtOH on autophagy flux. Thus, based on the changes in the number of GFP-LC3 dots, these data indicated that there were not only an increase in autophagosome synthesis but also an increase in autophagic degradation (Figures 4a and b). For further analysis of autophagosome maturation, we took advance of the mRFP-GFP-LC3 tandem reporter.[38] Administration of EtOH resulted in an increase of the percentage of autolysosomes (GFP−/RFP+ dots), being significative at high EtOH concentrations (from 200 mM; Figures 4c and d). p62 is a key adaptor molecule associated with selective autophagy: it binds to both LC3 and ubiquitinated autophagic substrates so that they could be taken up by the autophagosome for degradation. Therefore, decrease of p62 seen in western blot (Figures 3a and c) in EtOH-treated cells would support an enhanced autophagic degradation. Hence, our results strongly suggest that EtOH enhances autophagosome–lysosome fusion.

Autophagy can be cytoprotective or cytotoxic. Thus, EtOH-treated cells were also exposed to 3-methyl-adenine (3-MA), which inhibits autophagy. TUNEL analysis revealed an increase in the number of cell death in EtOH groups treated

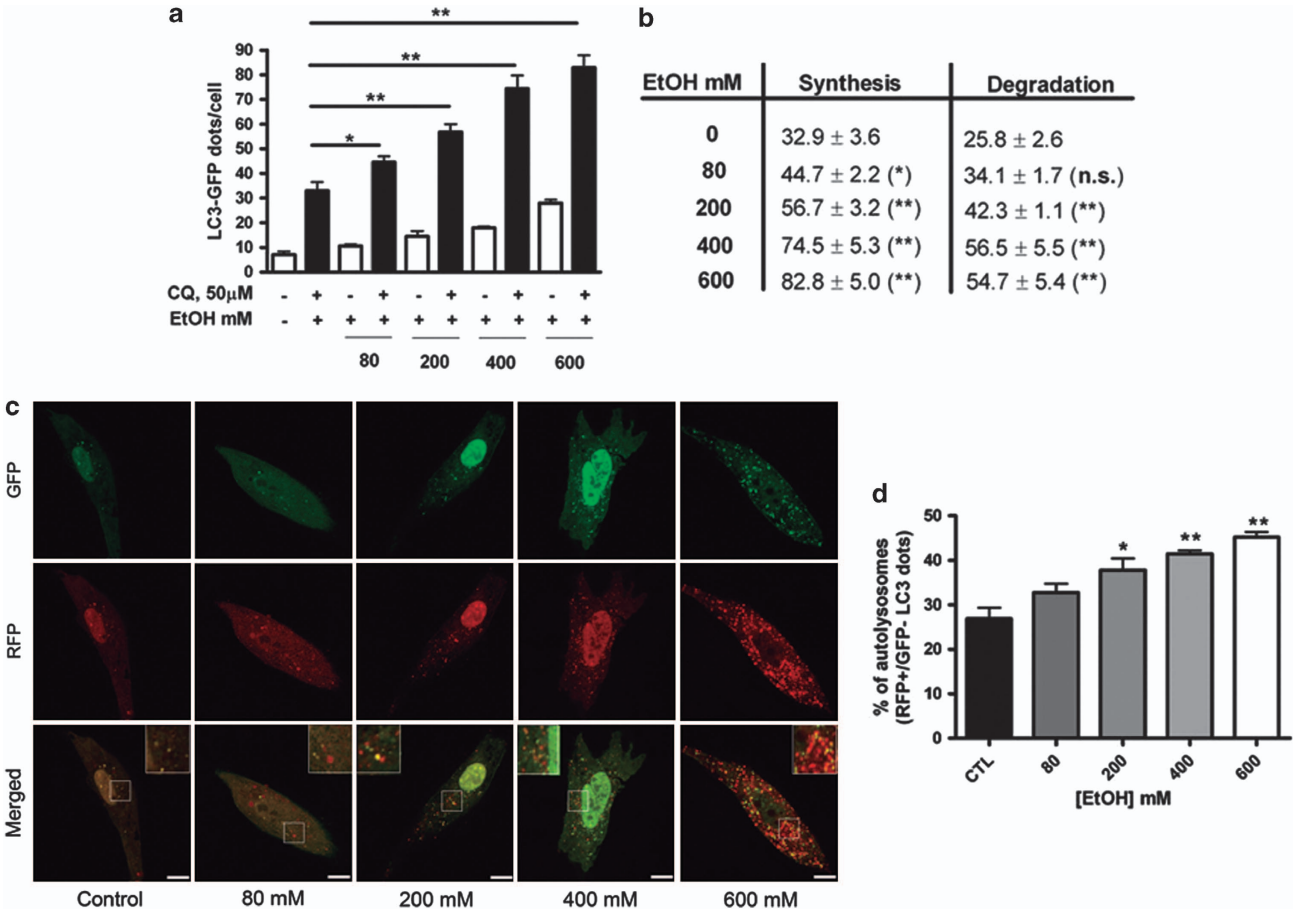

Figure 4 EtOH exposure increases autophagic flux. Cells were transfected with GFP-LC3 plasmid and treated or not with CQ and EtOH at different concentrations (80, 200, 400 and 600 mM). Histogram shows the number of LC3-GFP dots per cell (**a**). A summary of the autophagic flux values for synthesis and degradation is shown in table **b**. Confocal microscopy images of ARPE-19 cells transfected with mRFP-GFP-LC3 showing autophagosomes (yellow dots) and autolysosomes (red dots) (**c**). Quantification of autolysosomes (**d**). Values are expressed as mean ± S.E.M. ($N = 3$). Statistical significance was determined by a two-tailed Student's *t*-test (*$P < 0.05$ and **$P < 0.01$). Scale bars: 12 μm

with 3-MA (Figure 3k), more than twofold compared with EtOH groups alone. Our data propose autophagy has a cytoprotective role in EtOH-induced damage to ARPE-19 cells.

EtOH-induced mitochondrial fission and autophagic mitochondrial degradation. Mitochondrial morphology was analyzed by transfecting cells with the pDsRed2-Mito plasmid to express the DsRed2 protein fused to the mitochondrial targeting sequence of cytochrome c oxidase. After 24 h of transfection, untreated cultures presented mitochondria with long and tubular morphology (Figure 5a). EtOH exposure induced mitochondrial fragmentation and the formation of swollen, ball-shaped mitochondria in a concentration-dependent manner (Figure 5b) starting at 80 mM. Cell count of fragmented mitochondria is shown in Figure 5c.

Mitochondrial degradation by autophagy was observed in a concentration-dependent manner (Figures 5d–i). In fact, fragmented mitochondria were significantly closer to the autophagy vacuoles as EtOH concentration increased, overlapping finally with the autophagosome at 400 and 600 mM EtOH (Figures 5g and h). Incubation of cells with vinblastine (a microtubule-depolymerizing agent that induces accumulation of autophagic vacuoles by preventing their degradation) rendered a higher number of colocalizations of mitochondria and LC3 in the presence of EtOH (Figures 5j–l), which suggested a mitophagy increase, as observed before.[39]

EtOH altered redox status, increased lipid peroxidation and 4-HNE aggresomes. EtOH treatment significantly increased 2′,7′-dichlorofluorescein (DCFH) fluorescence levels in ARPE-19 cells compared with non-treated cells (Figure 6a), reflecting the 'redox status' of the cell. Consistently with these values, statistically significant increases of 4-HNE, 4-hydroxy-hexenal and malondialdehyde (MDA) were also observed with all EtOH concentrations in a dose-dependent manner (Figure 6b). Stressing the interest of both results was the highly significant positive correlation found between DCFH fluorescence and lipid peroxidation levels (Figure 6c).

Anti-4-HNE-immunocytochemistry was used to show the cellular location of the 4-HNE aggregates (Figures 7a and b), which were enhanced in number in a concentration-dependent manner, at every EtOH concentration (Figure 7c). 4-HNE-positive labeling was densely accumulated, forming large cytosolic ball-shaped aggregates (Figures 7d, g, j and m). We found that ARPE-19 cells exhibit a tendency to

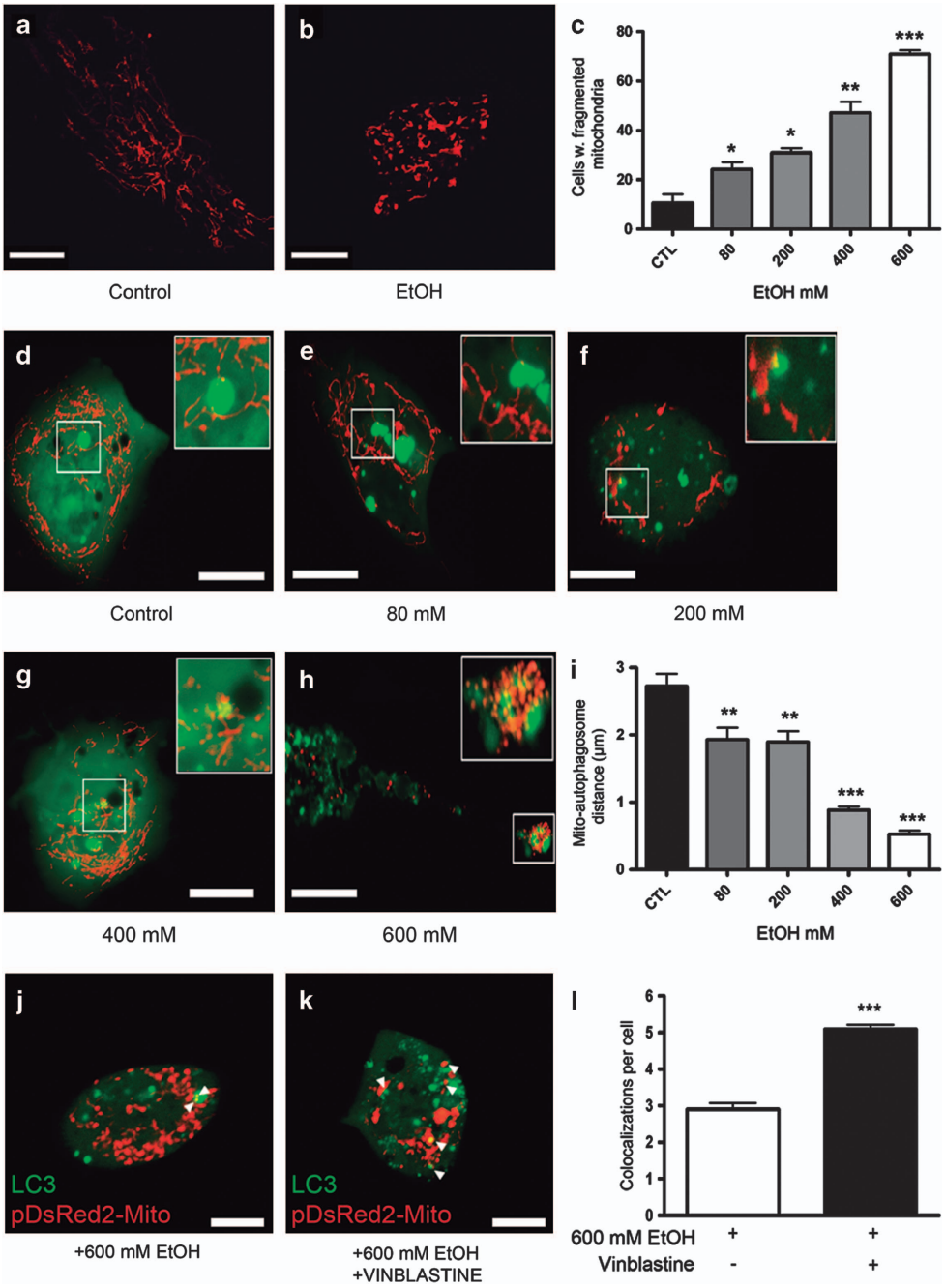

Figure 5 Mitochondrial fragmentation and distance to autophagosomes in ARPE-19 cells. ARPE-19 cells were transfected with pDsRed2-Mito plasmid. Mitochondrial morphology was observed in control (**a**) and 600 mM (**b**) EtOH in ARPE-19 cells. Histogram shows the percentage of cells with fragmented mitochondrial patterns (**c**). ARPE-19 cells were transfected with GFP-LC3 and pDsRed2-Mito plasmids. Expression of pDsRed2-Mito and GFP-LC3 plasmids was observed in control (**d**) and EtOH-treated cells at 80 mM (**e**), 200 mM (**f**), 400 mM (**g**) and 600 mM (**h**). Histogram shows the distance between mitochondria and autophagosome (**i**). Incubation with vinblastine of ARPE-19 cells. Colocalizations of mitochondria and LC3 in the presence of 600 mM EtOH in ARPE-19 cells (white arrows in **j** and **k**). Histogram shows the colocalizations per cell in the presence or absence of 10 μM vinblastine after 600 mM EtOH exposure (**l**). Values are expressed as mean ± S.E.M. ($N=3$). Statistical significance was determined by a two-tailed Student's *t*-test (*$P<0.05$, **$P<0.01$ and ***$P<0.001$). Scale bars: 12 μm

generate ubiquitin-positive, peri-nuclear inclusions that colocalize with 4-HNE (Figures 7d–f). Furthermore, the centrosome marker, γ-tubulin (Figures 7g–i) and the histone deacetylase 6 protein (HDAC6), also colocalized with 4-HNE aggregates (Figures 7j–l). Upon treatment of ARPE cells with nocodozole, a microtubule-depolymerizing agent, the perinuclear-localized inclusions failed to aggregate properly (Figures 7m and n). Taken together, 4-HNE-positive inclusions thus exhibit the classical hallmarks of aggresomes.[40]

Thus, the increase in the number of aggresomes could be a direct response to EtOH exposure or because EtOH disrupts

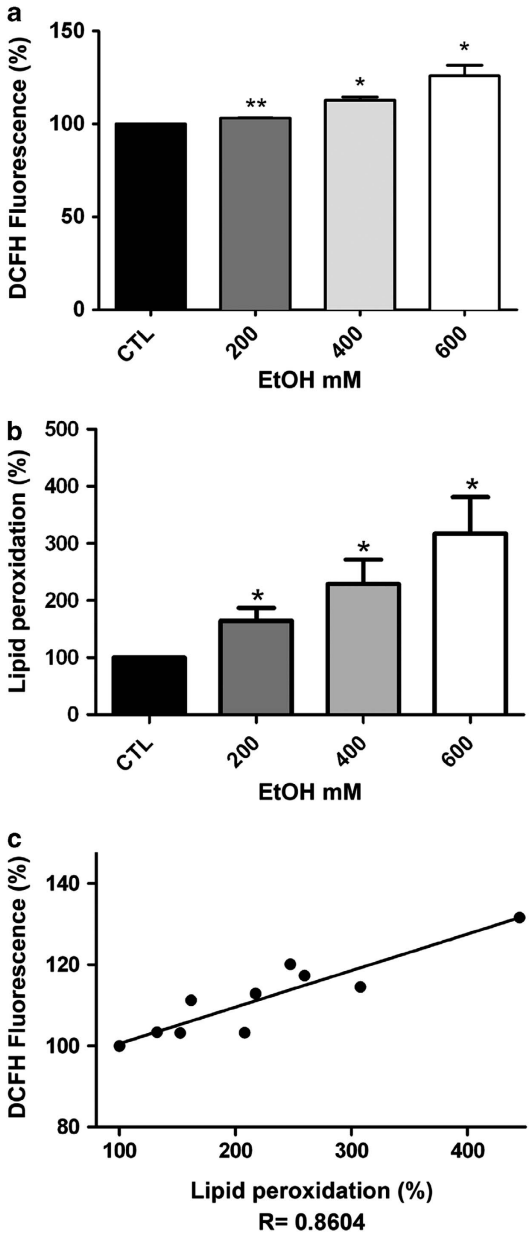

Figure 6 Determination of DCFH fluorescence and lipid peroxidation: HAE and MDA. Quantification of DCFH fluorescence (**a**) and lipid peroxidation (**b**) in control and EtOH-treated ARPE-19 cells. Positive correlation between DCFH fluorescence and lipid peroxidation (**c**). Values are expressed as mean ± S.E.M. ($N = 3$). Statistical significance was determined by one-way ANOVA test and Bonferroni analysis (*$P < 0.05$ and **$P < 0.01$)

somehow its degradation by autophagy. To solve this question, we first perform a double staining 4-HNE/LC3 observing colocalization (Figures 7o–q). Furthermore, the fact that after challenging EtOH-treated cells with 3-MA, the percentage of cells with 4-HNE perinuclear protein inclusions increased, clearly demonstrates that autophagy is capable of clearing 4-HNE aggresomes (Figure 7r).

EtOH induces ultrastructural changes. Significant morphological alterations were observed in semithin and ultrathin sections. Optical microscopy images revealed that untreated ARPE-19 cells exhibited a polyhedral shape, broad cytoplasm and nuclei that included lax chromatin with multiple nucleoli distributed along the nuclear matrix and nuclear invaginations (Figure 8a). Despite the fact that 600 mM EtOH-treated cells showed reduced cytoplasm, no differences in core size, number of nucleoli or nuclear invaginations could be established. EtOH-treated cells presented numerous vacuoles (arrows in Figure 8b), which were eventually associated with clusters (arrows in Figure 8c). Another recurring element in 600 mM EtOH-treated cells was a spherical area with less affinity for toluidine blue and a diameter of approximately 20 μm (asterisk in Figure 8d). In addition, some EtOH-treated cells showed partial absence of cytoplasmic organelles (arrow in Figure 8e). These observations were confirmed by electron microscopy. As expected, no differences in chromatin or nucleoli could be set. However, non-EtOH-treated cells often showed long mitochondria with extensive ramifications and dense matrices with tubular crests (arrows in Figure 8f), whereas mitochondria from EtOH-treated cells were more dilated, tended to be spherical-shaped and matrices were clear with fewer crests (arrows in Figure 8g). It is interesting to note that endoplasmic cisterns occasionally formed structures adjacent to mitochondria and dense bodies, sometimes observed surrounding them (Figure 8h). Another observed feature was the frequent presence of vacuoles with heterogeneous content in cells treated with 600 mM EtOH, varying greatly in electrodensity, with high electron-lucent and even multilamellar aspects (arrows in Figure 8i). Ultrastructural analysis demonstrated filamentous structures organized occasionally in masses tending toward sphericity but also in bundles distributed throughout the cytoplasm (arrows in Figure 8j). Some of these mitochondria presented an increased size and contained heterogeneous dense bodies with very irregular crests that hindered their identification as such (Figure 8k).

Discussion

We report here for the first time that EtOH exposure induces mitochondrial damage and protein aggregation in ARPE-19 cells. Furthermore, EtOH promotes flux of autophagy in order to decrease cellular toxicity induced by degrading fragmented mitochondria and protein inclusions.

ARPE-19 cells are particularly resistant to EtOH-induced toxicity. Using MTT assay as an approach to study the toxic effects of EtOH on ARPE-19 cells, we found that EtOH significantly increases toxicity at 600 mM EtOH. According to previous works on nervous cells, EtOH induces cell damage by the same technique at 140 mM.[14] This result, and the fact that EtOH increases ROS levels and lipid peroxidation products, agrees with previous reports, which indicated that ARPE-19 cells are extremely resistant to oxidative stress damage, when compared with other cell types. Furthermore, we also observed a slight decrease in cell proliferation after EtOH treatment,[4] Cell toxicity was also measured by the study of Bax, Bcl-2, and uncleaved caspase-3 protein expression. The anti-apoptotic protein Bcl-2 and pro-apoptotic Bax were elevated in a concentration-dependent manner, as well as uncleaved caspase-3 levels, which significantly

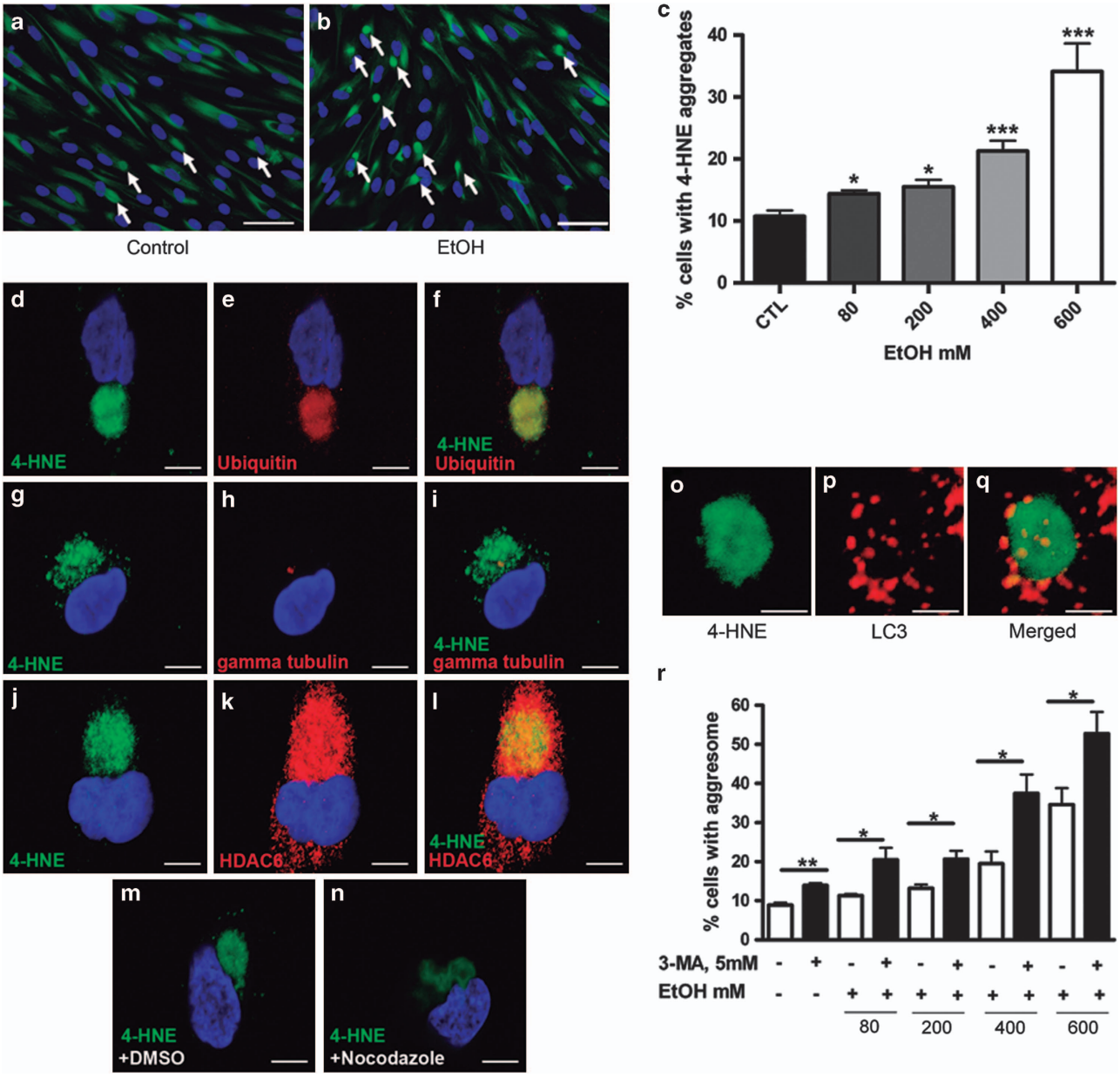

Figure 7 4-HNE aggresomes induced by EtOH and its degradation by autophagy in ARPE-19 cells. 4-HNE-positive cells (green) are indicated by white arrows in both untreated (**a**) and EtOH-treated ARPE-19 cells (**b**) after 24 h. Significant differences between control and treated cells are observed at different concentrations (**c**). 4-HNE-positive labeling was densely accumulated forming large ball-shaped aggregates in the vicinity of the nucleus (**d, g** and **j**). Ubiquitin (**e**), gamma tubulin (**h**) and HDAC6 (**k**) positive labeling (red). Colocalization of 4-HNE with ubiquitin (**f**), gamma tubulin (**i**) and HDAC6 (**l**). 4-HNE-positive labeling in the presence of the solvent DMSO (**m**) and Nocodazole (1 μg/ml) (**n**). 4-HNE aggregate colocalize with LC3 dots after EtOH exposure (**o–q**). Cells were challenged with or without EtOH and 3-MA, after fixation 4-HNE immunostaining was performed. Histogram shows the percentage of cells with 4-HNE inclusion with or without EtOH and 3-MA exposure (**r**). Values are expressed as mean ± S.E.M. ($N = 3$). Statistical significance was determined by a two-tailed Student's *t*-test (*$P < 0.05$; **$P < 0.01$; ***$P < 0.001$). Scale bars on (**a**, **b**): 50 μm; (**d–q**): 12 μm

increases at 600 mM. Surprisingly, no significant cell death could be established at 600 mM by flow cytometry. However, TUNEL analysis showed a small but significant increase in cell death only at 600 mM of EtOH, although the number of degenerated cells was still very low (around 3.5% more than controls).

EtOH treatment activates autophagy in ARPE-19 cells. Electron microscopy analysis confirmed the presence of increased autophagic vacuoles induced by EtOH. These autophagic vacuoles presented heterogeneous structures with similar content to those described by others.[41,42] Autophagosome content was significantly increased at every EtOH concentration in a concentration-dependent manner, starting at 80 mM, a concentration normally used to study autophagy under EtOH damage in other cell lines.[14,15] This evidence was supported by the fact that EtOH promoted the formation of LC3-II as well as increased the number of GFP-LC3 dots per cell and the number of autophagic cells. Our data also indicated that the increase in the number of

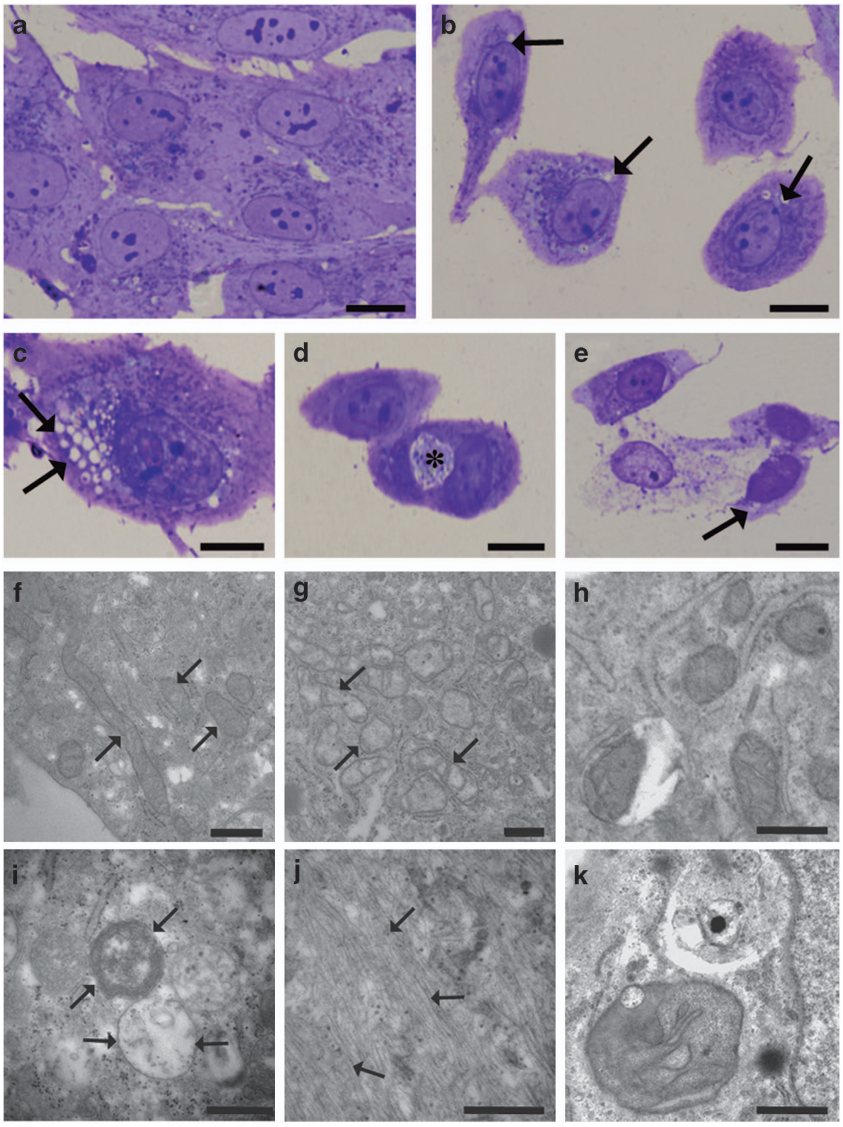

Figure 8 Optical and transmission electron microscopy in ARPE-19 cells. Nuclei of control cells with lax chromatin and multiple nucleoli (**a**). EtOH-treated cells at 600 mM show reduced cytoplasm and numerous vacuoles (arrows in **b**). Vacuoles can aggregate as clusters (arrows in **c**). Asterisk corresponds to a spherical area with less affinity for toluidine blue (**d**). Eventually, some EtOH-treated cells show absence of cytoplasm organelles (arrow in **e**). Under the electron microscope, control cells present long mitochondria with dense matrices and tubular crests (arrows in **f**). EtOH-treated cells present dilated mitochondria and spherical shape (arrows in **g**). Mitochondria inside vesicles next to ER were also observed (**h**). Vacuoles with heterogeneous content (arrows in **i**) and filamentous structures (arrows in **j**). Mitochondria show heterogeneous dense bodies and irregular crests (**k**) close to a double membrane vesicle. Scale bars: **a–e**: 25 μm; **f–j**: 0,5 μm; **k**: 1 μm

autophagosomes was related to an increase of autophagic flux (synthesis and degradation) rather than a decrease in autophagosome–lysosome fusion as previously reported in HepG2 cells.[43] Autophagy flux analysis revealed that EtOH promotes autophagosome synthesis in a concentration-dependent manner as well as autophagosome degradation. Furthermore, EtOH decreases p62 levels, a key adaptor molecule associated with selective autophagy: it binds to both LC3 and ubiquitinated autophagic substrates so that they could be taken up by the autophagosome for degradation. EtOH treatment also increases the percentage of GFP$-$/RFP$+$ dots. These two evidences demonstrated that EtOH increases autophagosome degradation by fusion with the lysosome. Although autophagosome synthesis is increased from 80 mM, autophagosome to lysosome fusion significantly increased only at high EtOH concentrations (above 200 mM). Our results are in agreement with previous works reporting that EtOH increases autophagy flux in liver and brain cells.[14,15]

EtOH exposure induces mitochondrial fragmentation and promotes mitophagy. The negative effects of EtOH on hepatic[44–46] and neuronal[47] mitochondria are well documented. Here, we report for the first time changes in ARPE-19 mitochondrial morphology following EtOH exposure leading to an increase of mitochondrial fragmentation in a concentration-dependent manner at every EtOH concentration, in agreement with previous works in liver and brain

cells.[14,15] Furthermore, electron microscopy analysis also indicated a loss of normal mitochondrial morphology, tended to spherical and a loss of mitochondrial crests, confirming mitochondrial damage induced by EtOH. As reported before, one of the most interesting forms of autophagy is the one related to the degradation of fragmented mitochondria. Interestingly, we observed a reduction in the distance between autophagosomes and fragmented mitochondria that could be a prelude for mitophagy. Some of the most important changes after EtOH exposure are the mitochondrial morphology alterations, the lack of crests and the presence of heterogeneous bodies surrounded by ER. This is relevant because the ER–mitochondria contact site has been suggested to be a key point to promote autophagy.[48] Moreover, mitochondria inside vesicles were also observed. Besides, by using vinblastine (a microtubule-depolymerizing agent that induces accumulation of autophagic vacuoles by preventing their degradation, as mentioned above) we observed an increase of autophagosome–mitochondria colocalization. This observation, together with the mitochondria–autophagosome approximation, the unusual over-sized mitochondria with heterogeneous dense bodies, and the fact that mitochondria supply membranes for autophagosome genesis[49] strongly suggest the occurrence of EtOH-induced mitophagosomes in ARPE-19 cells, in agreement with previous studies carried out in liver.[50,51]

EtOH promotes protein aggregation and increases aggrephagy. 4-HNE is a good marker of lipid peroxidation, and its ability to form protein adducts has been demonstrated in human brain of PD patients[52] as well as in hepatocytes after EtOH exposure.[30] In addition, it has been shown that 4-HNE forms adducts with the proteasome subunits that are responsible for proteasomal activity inhibition in liver.[28] Unspecific spherical areas (described in Figure 7d) correspond to the 4-HNE aggregates, which can be classified for the first time as aggresomes. Misfolded ubiquitinated proteins that cannot be degraded by the proteasome system are driven by the HDAC6, which recognizes the ubiquitin residue through microtubules to the aggresome, localized around the centrosome.[40] Hence, the fact that 4-HNE colocalizes with ubiquitin, gamma-tubulin and HDAC6, and requires microtubules for its correct formation clearly demonstrated the aggresome nature of these 4-HNE aggregates. As reported previously,[28] aggresomes could be degraded by autophagy depending on the proteins aggregated. The fact that 4-HNE colocalizes with LC3, and that 3-MA (an autophagy inhibitor) increases the percentage of cells with 4-HNE aggresomes strongly suggest that EtOH increases aggresome degradation by autophagy (aggrephagy), and that EtOH does not alter autophagosome cargo recognition, as observed in a model of HD.[53] Interestingly, Cuervo's group indicated that in their cell model, aggrephagy cannot be produced without inducing autophagy.[39] However, in our model we found that control cells normally degrade 4-HNE inclusions. This can be due to the high autophagy levels observed in control ARPE-19 cells previously reported.[4] Therefore, ARPE-19 cells are able to degrade damaged organelles without inducing autophagy.

Autophagy has a cytoprotective role in EtOH-induced toxicity in ARPE-19 cells. Autophagy is a catabolic process, which has a cytoprotective role under oxidative conditions in most of the cases. However, a hyperactivation of autophagy can lead to cell death.[54] Previous data demonstrated that autophagy formation attenuated EtOH-induced damage in liver[15,51] and neuroblastoma cells.[14] It has been shown that autophagy inhibition enhanced EtOH-induced ROS production and neurotoxicity,[15] presumably due to the lack of clearance of damaged mitochondria and misfolded proteins. Thus, fragmented mitochondria are toxic for the cell, as well as aggresomes. Furthermore, after EtOH treatment, mitophagy and aggrephagy are enhanced. Therefore, we could hypothesize that autophagy promotes cell survival in ARPE-19 cells under EtOH exposure. Moreover, autophagy inhibition by 3-MA increases cell death (more than twofold) in EtOH-treated cells. Thus, our results strongly suggest that autophagy, by degrading fragmented mitochondria and protein inclusions, reduces cell toxicity produced by EtOH.

The present work reveals, for the first time, the existence of 4-HNE aggresomes induced by EtOH, without connection to any protein mutation (observed in PD, HD or AD). These data open new questions about the role of 4-HNE in protein aggregation. Interestingly, accumulation of aggresomes has been observed in post-mortem neurological histological preparations as indicators of chronic alcoholism.[32] We also demonstrate that EtOH exposure induces mitochondrial fragmentation that leads to mitophagy in ARPE-19 cells. Both results are consistent with the effects of EtOH in brain cells.[10] Furthermore, mitochondrial damage, protein aggregation and autophagy activation seem to be crucial processes in a RPE-related disease like AMD.[55,56] Considering that aggresomes are of relevance in neuropathology as much as mitochondrial fragmentation,[57] our results describing a neurodegenerative-like phenotype in ARPE-19 cells induced by EtOH are novel and deserve further research, as they may contribute to the better understanding of the pathophysiological mechanism of other neurodegenerative diseases, including the formerly proposed 'alcoholic retinopathy'.[12]

Materials and Methods

Cell culture. Human retinal pigment epithelial cell line ARPE-19 was obtained from American Type Culture Collection (ATCC, Barcelona, Spain). ARPE-19 cells were cultured in Dulbecco's modified Eagle's medium/Nutrient mixture F12 (DMEM/F12, Invitrogen, Grand Island, NY, USA) supplemented with 5 mM HEPES buffer, 7.5% $NaHCO_3$, 10% fetal bovine serum and 1% penicillin/streptomycin and were maintained at 37 °C and 5% CO_2. Cells were used from 18 to 20 passages and cultivated in six-cell culture well plates at a starting seeding density of 2×10^5 cells/cm^2. Two days after, cells were treated for 24 h at different EtOH (Ethanol absolute; Biosolve, Valkenswaard, The Netherlands) concentrations: 80, 200, 400 and 600 mM.

MTT assay. The 3-(4,5-dimethylthiazol-2-yl)-2,5-diphenyltetrazolium bromide (MTT) assay (Cell Proliferation Kit I; Roche, Mannheim, Germany) was used to determine cell proliferation in terms of mitochondrial activity. ARPE-19 cells were seeded at 1×10^4 per well in a 96-cell culture well plate and grew to confluence for 24 h. Cells were treated with EtOH at different concentrations for 24 h. MTT labeling reagent (0.5 mg/ml) was added to each well and incubated for 4 h at 37 °C in 5% CO_2. Then, solubilization solution was added and incubated overnight at 37 °C in 5% CO_2. Absorbance was read at 550 nm by microplate reader (Victor 3; Perkin Elmer, Turku, Finland). Each treatment condition was repeated 10 times.

Flow cytometric analysis using V-FITC and PI staining. ARPE-19 cells were resuspended in 200 μl Annexin binding buffer at 200×10^5 cells/ml, V-FITC and PI solution were added. Then, samples were diluted with 400 μl binding buffer and analyzed with a FACScan flow cytometer (FACScan; Beckman Coulter, Brea, CA, USA). Ten thousand events were collected for each sample. Results were analyzed with BD FAC Suite software (Fullerton, CA, USA).

Determination of lipid peroxidation: hydroxyalkenals and MDA. Lipid peroxides are unstable and decompose to form a complex series of compounds, including MDA and HAE, upon decomposition, and the measurement of MDA and HAE has been used as an indicator of lipid peroxidation. MDA and HAE were determined by using the Lipid Peroxidation Microplate Assay Kit (Oxford Biomedical Research, Bicester, Oxfordshire, UK). Briefly, ARPE-19 cells were treated with EtOH for 24 h. Absorbance of the stable yielded chromophore was measured at 586 nm with a multiplate reader (Victor 3; Perkin Elmer).

Determination of ROS levels. ROS levels were measured using 2′7′-dichlorodihydrofluorescein diacetate (H2DCFDA; Santa Cruz Biotechnology, Santa Cruz, CA, USA), which is converted to a non-fluorescent derivative (H2DCF) by intracellular esterases. This molecule can be oxidized by ROS producing intracellular dichlorofluorescein (DCF), which is a fluorescent compound. Cells were incubated with 15 μM of H2DCFDA for 15 min at 37 °C. Intracellular ROS production was measured by fluorescence multiplate reader (Victor X5; Perkin Elmer) excited at 485 nm and read at 530 nm.

Western blot analysis. Cells were subsequently scraped with ice-cold PBS and lysed with RIPA buffer (Sigma-Aldrich, St. Louis , MO, USA) containing 50 mM Tris-HCl, pH 8.0, 150 mM sodium chloride, 1.0% Igepal CA-630 (NP-40), 0.5% sodium deoxycholate, 0.1% sodium dodecyl sulfate and Protease Inhibitor Cocktail (Sigma-Aldrich). Equal amount of protein from each sample (35 μg) was measured by SDS-PAGE on 4–12% gels and electroblotted onto polyvinylidene difluoride membranes (Millipore, Billerica, MA, USA). Membranes were incubated overnight at 4 °C with a rabbit polyclonal antibody against uncleaved caspase-3 (1 : 500; Santa Cruz Biotechnology), Bax (1 : 250; Santa Cruz Biotechnology), Bcl-2 (1 : 500; Santa Cruz Biotechnology), LC3 (1 : 1000; Sigma-Aldrich) and mouse monoclonal antibody against β-actin (1 : 500; Santa Cruz Biotechnology), GAPDH (1 : 1000; Santa Cruz Biotechnology) and p62 (1 : 1000; Cell Signaling, Danvers, MA, USA). Subsequently, membranes were incubated 2 h at room temperature in horseradish peroxidase-conjugated anti-mouse and anti-rabbit IgG (1 : 10 000; Santa Cruz Biotechnology). Bands were visualized with ECL (Pierce, Thermo Scientific, Rockford, IL, USA) and detected with Image Quant LAS-4000 mini (GE Healthcare, Uppsala, Sweden). Protein levels were quantified by densitometry using ImageJ software (National Institutes of Health, Bethesda, MD, USA). Protein expression intensity was normalized to β-actin or GAPDH.

TUNEL assay. The TUNEL assay is performed using an *in situ* cell death detection kit conjugated with tetra-methyl-rhodamine or fluorescein isothiocyanate (Roche). For controls, terminal deoxynucleotidyl transferase enzyme is either omitted from the labeling solution (negative control), or sections are pretreated for 30 min with DNAse I (Roche; 3 U/ml) in 50 mM Tris-HCl, pH 7.5, 1 mg/ml BSA to induce DNA-strand breaks (positive control).

Immunocytochemistry. Cells were incubated overnight with primary antibody: anti-4-HNE (1 : 200; Abcam, Cambridge, MA, USA), anti-Ki-67 (1 : 100; Sigma-Aldrich), anti-ubiquitin (1 : 50; Santa Cruz Biotechnology) and anti-HDAC6 (1 : 100; Santa Cruz Biotechnology) at 4 °C. Afterward, cells were incubated with fluorescent-conjugated secondary antibodies Alexa Fluor 555 goat anti-rabbit IgG, Alexa Fluor 488 goat anti mouse IgG (1 : 500; Molecular Probes, Invitrogen, Carlsbad, CA, USA) for 1 h at room temperature. Finally, for DNA staining, cells were incubated for 10 min with 4,6-diamidino-2-phenylindole (DAPI; Sigma-Aldrich). Fluorescence images were recorded with a laser scanning microscope (LSM 710) and the ZEN Software from Carl Zeiss AG (Oberkochen, Germany).

Autophagosome analysis. As previously described, GFP-LC3 can be used to monitor the presence of autophagosomes.[58] A subset of GFP-LC3 is localized on the autophagosome membrane, hence, the presence of GFP-LC3 puncta (dots) by fluorescence microscopy indicates the presence of autophagosomes. Autophagy was measured by quantifying the percentage of cells with punctate GFP-LC3 (autophagic cells). In fact, cells with more than nine autophagosomes were counted as autophagic. At least 200 transfected cells were counted for each condition. In addition, the total number of GFP-LC3 dots per cell was also measured, in at least 30 transfected cells per condition. To study the effect of EtOH on autophagosome maturation, ARPE-19 cells were transfected with an mRFP-GFP-LC3 tandem reporter that has been found to be useful to trace autophagosome maturation.[59] Hence, within lysosomes GFP-LC3 fluorescence was quenched because of the sensitivity of GFP to acidic environments, whereas mRFP-LC3 fluorescence was more stable upon acidification. Thus, autophagosomes with a physiological pH show both red and green fluorescence (yellow dots), whereas the latter was lost in autolysosomes with an acidic pH (red dots). After overlapping images in both channels, the number of LC3 dots in each cell was analyzed: RFP + /GFP + (yellow) dots as autophagosomes and RFP + / GFP − (red) dots as autolysosomes. Therefore, the percentage of red dots (RFP + /GFP −) in each cell is a measure of the number of autolysosomes.[59] At least, 30 transfected cells were counted for each condition. Cells were viewed under a laser scanning microscope (LSM 170; Carl Zeiss).

Transfections. Twenty-four hours before transfection, cells were plated at a density of 5×10^4 cells/cm^2 on IBIDI-coated glass dishes. Transfection was achieved using Lipofectamine 2000 reagent (Invitrogen) according to the manufacturer's protocol. Cells were transfected with the different plasmids and after 4-h incubation, transfection mixture was removed and replaced with fresh complete medium. The pDsRed2 plasmid was purchased from Clontech (BD Biosciences, San Jose, CA, USA). GFP-LC3 is a gift from Dr JM Fuentes (Universidad de Extremadura, Spain) and mRFP-GFP-LC3 from Dr Erwin Knecht (Centro de Investigación Príncipe Felipe, Spain).

Analysis of mitochondrial morphology. Cells were transfected with pDsRed2-Mito plasmid, which leads to the expression of fluorescent DsRed2 in mitochondria, thereby labeling the organelles. The transfected cells were subjected to experimental treatments, and mitochondrial morphology was evaluated by fluorescence microscopy. For quantification, the percentage of cells with abnormal mitochondrial morphologies was determined and taken as a measure of the proportion of cells with fragmented mitochondria. Fluorescence images were recorded with a laser scanning microscope (LSM 710) and the ZEN Software from Carl Zeiss AG.

Autophagic flux assay. Autophagy flux was analyzed based on methods described.[15,60] The synthesis was defined as the values of 'EtOH + CQ' and 'Control + CQ', whereas degradation was defined as the difference between the values of 'Control + CQ' and 'Control only' (without CQ), and between the values of 'EtOH + CQ' and 'EtOH only' (treatment without CQ). Thus, the synthesis measures the increase of GFP-LC3 dots or autophagosomes, stimulated by the treatment while in the presence of CQ (which clamps the degradation). A higher value of 'EtOH + CQ' compared with 'Control + CQ' indicates a net increase in these parameters, thus suggesting a promotion of autophagy process. The degradation, assuming at steady state, measures the increase caused by CQ, which otherwise would be degraded in the absence of CQ. If the values of degradation in the EtOH group ('EtOH + CQ'–'EtOH only') are higher than those in the Control group ('Control + CQ'–'Control only'), it may be inferred that the treatment used promotes autophagy degradation.

Inclusion formation and autophagic clearance. The susceptibility of 4-HNE inclusions formed upon EtOH treatment toward autophagic removal was analyzed as previously described.[39] Briefly, cells were challenged with EtOH (80, 200, 400 and 600 mM) either in the presence or absence of the autophagy inhibitor, 5 mM 3-MA (Sigma-Aldrich). Thus, an increase in the percentage of cells with 4-HNE inclusions in the presence of 3-MA would suggest that 4-HNE aggresomes are cleared by autophagy.

Electron microscopy. ARPE-19 cells were seeded at a density of 3×10^4 cells per well in eight-well Lab-Tek chamber slides (Nalge Nunc Int., Roskilde, Denmark) and fixed in 3.5% glutaraldehyde for 1 h at 37 °C. The cells were then postfixed in 2% OsO_4 for 1 h at room temperature and stained with 2% uranyl acetate in the dark for 2 h at 4 °C. Finally, cells were rinsed in 0.1 M PBS, dehydrated in EtOH, and infiltrated overnight with Araldite (Durcupan, Fluka, Heidelberg, Germany). Following polymerization, embedded cultures were detached from the chamber slide and glued to araldite blocks. Serial semithin (1.5 μm) sections were cut with an Ultracut UC-6 microtome (Leica Microsystems,

Wetzlar, Germany), mounted onto slides and stained with 1% toluidine blue (optical microscopy). Selected sections were glued (Super Glue, Loctite, Westlake, OH, USA) to araldite blocks and detached from the glass slide by repeated freezing (in liquid nitrogen) and thawing. Ultrathin (0.06–0.09 μm) sections were prepared on the Ultracut microtome and stained with lead citrate. Finally, photomicrographs were obtained using a transmission electron microscope (FEI Tecnai G2 Spirit Biotwin, Hillsboro, OR, USA) coupled to an Olympus digital camera (Olympus, Tokyo, Japan). Electron microscopy experiments were performed in triplicate and the analysis of the samples was performed in a blind manner.

Statistical analysis. Statistical analysis was done using SPSS 15 software (IBM, Armonk, NY, USA). Lipid peroxidation, ROS, MTT, immunocytochemistry, autophagic vacuole density, mitochondrial fragmentation and distance measures to autophagic vacuoles analysis comparisons were performed using one- and two-way ANOVA, Bonferroni analysis and Student's two-tailed unpaired *t*-test. Statistical differences were set at $P<0.05$.

Conflict of Interest

The authors declare no conflict of interest.

Acknowledgements. We thank Carlos Bueno-Beti (LINCE, UV) for his assistance with the FACScan flow cytometer; and Leticia Gómez de Manuel and Diana Martinez for excellent technical assistance. We thank Dr Knecht (Laboratory of Cellular Biology, Centro de Investigación Príncipe Felipe (CIPF)) for kindly providing the mRFP-GFP-LC3 plasmid. We also would like to acknowledge Patricia García Tarraga and Mario Soriano Navarro for their technical support at the CIPF Transmission Electron Microscopy. This study was supported in part by a grant from the Ministerio de Ciencia e Innovación, Spain (SAF2010-21317) and funds from the Universidad Católica de Valencia to FJR.

1. Reichenbach A, Pritz-Hohmeier S. Normal and disturbed early development of the eye anlagen. *Prog Retin Eye Res* 1995; **14**: 1–45.
2. Strauss O, Stumpff F, Mergler S, Wienrich M, Wiederholt M. The Royal College of Surgeons rat: an animal model for inherited retinal degeneration with a still unknown genetic defect. *Acta Anat* 1998; **162**: 101–111.
3. Winkler BS, Boulton ME, Gottsch JD, Sternberg P. Oxidative damage and age- related macular degeneration. *Mol Vis* 1999; **5**: 32.
4. Kurz T, Karlsson M, Brunk UT, Nilsson SE, Frennesson C. ARPE-19 retinal pigment epithelial cells are highly resistant to oxidative stress and exercise strict control over their lysosomal redox-active iron. *Autophagy* 2009; **5**: 494–501.
5. Strauss O. The retinal pigment epithelium in visual function. *Physiol Rev* 2005; **85**: 845–881.
6. Giansanti V, Rodriguez GE, Savoldelli M, Gioia R, Forlino A, Mazzini G *et al.* Characterization of stress response in human retinal epithelial cells. *J Cell Mol Med* 2013; **17**: 103–115.
7. Kim JY, Zhao H, Martinez J, Doggett TA, Kolesnikov AV, Tang PH *et al.* Noncanonical autophagy promotes the visual cycle. *Cell* 2013; **154**: 365–376.
8. Ferguson TA, Green DR. Autophagy and phagocytosis converge for better vision. *Autophagy* 2014; **10**: 165–167.
9. Miller L, Shapiro AM, Cheng J, Wells PG. The free radical spin trapping agent phenylbutylnitrone reduces fetal brain DNA oxidation and postnatal cognitive deficits caused by in utero exposure to a non-structurally teratogenic dose of ethanol: a role for oxidative stress. *Free Radic Biol Med* 2013; **60**: 223–232.
10. Haorah J, Ramirez SH, Floreani N, Gorantla S, Morsey B, Persidsky Y. Mechanism of alcohol-induced oxidative stress and neuronal injury. *Free Radic Biol Med* 2008; **45**: 1542–1550.
11. Herrera DG, Yague AG, Johnsen-Soriano S, Bosch-Morell F, Collado-Morente L, Muriach M *et al.* Selective impairment of hippocampal neurogenesis by chronic alcoholism: protective effects of an antioxidant. *Proc Natl Acad Sci USA* 2003; **100**: 7919–7924.
12. Sancho-Tello M, Muriach M, Barcia J, Bosch-Morell F, Genovés JM, Johnsen- Soriano S *et al.* Chronic alcohol feeding induces biochemical, histological, and functional alterations in rat retina. *Alcohol Alcohol* 2008; **43**: 254–260.
13. Johnsen-Soriano S, Bosch-Morell F, Miranda M, Asensio S, Barcia JM, Romá J *et al.* Ebselen prevents chronic alcohol-induced rat hippocampal stress and functional impairment. *Alcohol Clin Exp Res* 2007; **31**: 486–492.
14. Chen G, Ke Z, Xu M, Liao M, Wang X, Qi Y *et al.* Autophagy is a protective response to ethanol neurotoxicity. *Autophagy* 2012; **8**: 1577–1589.
15. Ding WX, Li M, Chen X, Ni HM, Lin CW, Gao W *et al.* Autophagy reduces acute ethanol-induced hepatotoxicity and steatosis in mice. *Gastroenterology* 2010; **139**: 1740–1752.
16. Karunadharma PP, Nordgaard CL, Olsen TW, Ferrington DA, Mitochondrial DNA. damage as a potential mechanism for age-related macular degeneration. *Invest Ophthalmol Vis Sci* 2010; **5**: 5470–5479.
17. Lin H, Qian J, Castillo AC, Long B, Keyes KT, Chen G *et al.* Effect of miR-23 on oxidant-induced injury in human retinal pigment epithelial cells. *Invest Ophthalmol Vis Sci* 2011; **52**: 6308–6314.
18. Youle RJ, Narendra DP. Mechanisms of mitophagy. *Nat Rev Mol Cell Biol* 2011; **12**: 9–14.
19. Cohen G, Riahi Y, Sunda V, Deplano S, Chatgilialoglu C, Ferreri C *et al.* Signaling properties of 4-hydroxyalkenals formed by lipid peroxidation in diabetes. *Free Radic Biol Med* 2013; **65**: 978–987.
20. Dalleau S, Baradat M, Guéraud F, Huc L. Cell death and diseases related to oxidative stress: 4-hydroxynonenal (HNE) in the balance. *Cell Death Differ* 2013; **20**: 1615–1630.
21. Kaarniranta K, Ryhänen T, Karjalainen HM, Lammi MJ, Suuronen T, Huhtala A *et al.* Geldanamycin increases 4-hydroxynonenal (HNE)-induced cell death in human retinal pigment epithelial cells. *Neurosci Lett* 2005; **382**: 185–190.
22. Johnston JA, Ward CL, Kopito RR. Aggresomes: a cellular response to misfolded proteins. *J Cell Biol* 1998; **143**: 1883–1898.
23. Siegel SJ, Bieschke J, Powers ET, Kelly JW. The oxidative stress metabolite 4- hydroxynonenal promotes Alzheimer protofibril formation. *Biochemistry* 2007; **46**: 1503–1510.
24. Lee J, Kosaras B, Del Signore SJ, Cormier K, McKee A, Ratan RR *et al.* Modulation of lipid peroxidation and mitochondrial function improves neuropathology in Huntington's disease mice. *Acta Neuropathol* 2011; **121**: 487–498.
25. Sekigawa A, Fujita M, Sekiyama K, Takamatsu Y, Hatano T, Rockenstein E *et al.* Distinct mechanisms of axonal globule formation in mice expressing human wild type α-synuclein or dementia with Lewy bodies-linked P123H β-synuclein. *Mol Brain* 2012; **5**: 34.
26. Ross CA, Poirier MA. Protein aggregation and neurodegenerative disease. *Nat Med* 2004; **10**(Suppl): 10–17.
27. Wong ES, Tan JM, Soong WE, Hussein K, Nukina N, Dawson VL *et al.* Autophagy-mediated clearance of aggresomes is not a universal phenomenon. *Hum Mol Genet* 2008; **17**: 2570–2582.
28. Wong E, Cuervo AM. Autophagy gone awry in neurodegenerative diseases. *Nat Neurosci* 2010; **13**: 805–811.
29. Harris H, Rubinsztein DC. Control of autophagy as a therapy for neurodegenerative disease. *Nat Rev Neurol* 2011; **8**: 108–117.
30. Amidi F, French BA, Chung D, Halsted CH, Medici V, French SW. M-30 and 4HNE are sequestered in different aggresomes in the same hepatocytes. *Exp Mol Pathol* 2007; **83**: 296–300.
31. Bardag-Gorce F, French BA, Nan L, Song H, Nguyen SK, Yong H *et al.* CYP2E1 induced by ethanol causes oxidative stress, proteasome inhibition and cytokeratin aggresome (Mallory body-like) formation. *Exp Mol Pathol* 2006; **81**: 191–201.
32. Laas R, Hagel C. Hirano bodies and chronic alcoholism. *Neuropathol Appl Neurobiol* 1994; **20**: 12–21.
33. Eriksson AK, Löfving S, Callaghan RC, Allebeck P. Alcohol use disorders and risk of Parkinson's disease: findings from a Swedish national cohort study 1972-2008. *BMC Neurol* 2013; **5**: 190.
34. Van der Mark M, Nijssen PC, Vlaanderen J, Huss A, Mulleners WM, Sas AM *et al.* A case-control study of the protective effect of alcohol, coffee, and cigarette consumption on Parkinson disease risk: time-since-cessation modifies the effect of tobacco smoking. *PLoS One* 2014; **9**: e95297.
35. Brossas JY, Tanguy R, Brignole-Baudouin F, Courtois Y, Torriglia A. Tréton J. L- DNase II associated with active process during ethanol induced cell death in ARPE-19. *Mol Vis* 2004; **10**: 65–73.
36. Reggiori F, Monastyrska I, Verheije MH, Calì T, Ulasli M, Bianchi S *et al.* Coronaviruses Hijack the LC3-I-positive EDEMosomes, ER-derived vesicles exporting short-lived ERAD regulators, for replication. *Cell Host Microbe* 2010; **7**: 500–508.
37. Bernasconi R, Galli C, Noack J, Bianchi S, de Haan CA, Reggiori F *et al.* Role of the SEL1L:LC3-I complex as an ERAD tuning receptor in the mammalian ER. *Mol Cell* 2012; **46**: 809–819.
38. Kimura S, Noda T, Yoshimori T. Dissection of the autophagosome maturation process by a novel reporter protein, tandem fluorescent-tagged LC3. *Autophagy* 2007; **3**: 452–460.
39. Wong E, Bejarano E, Rakshit M, Lee K, Hanson HH, Zaarur N *et al.* Molecular determinants of selective clearance of protein inclusions by autophagy. *Nat Commun* 2012; **3**: 1240.
40. Kawaguchi Y, Kovacs JJ, McLaurin A, Vance JM, Ito A, Yao TP. The deacetylase HDAC6 regulates aggresome formation and cell viability in response to misfolded protein stress. *Cell* 2003; **115**: 727–738.
41. Sansanwal P, Yen B, Gahl WA, Ma Y, Ying L, Wong LJ *et al.* Mitochondrial autophagy promotes cellular injury in nephropathic cystinosis. *J Am Soc Nephrol* 2010; **21**: 272–283.
42. Zhang Q, Yang YJ, Wang H, Dong QT, Wang TJ, Qian HY *et al.* Autophagy activation: a novel mechanism of atorvastatin to protect mesenchymal stem cells from hypoxia and serum deprivation via AMP-activated protein kinase/mammalian target of rapamycin pathway. *Stem Cells Dev* 2012; **21**: 1321–1332.
43. Thomes PG, Ehlers RA, Trambly CS, Clemens DL, Fox HS, Tuma DJ *et al.* Multilevel regulation of autophagosome content by ethanol oxidation in HepG2 cells. *Autophagy* 2013; **9**: 63–73.
44. Cederbaum AI, Lieber CS, Rubin E. Effects of chronic ethanol treatment of mitochondrial functions damage to coupling site I. *Arch Biochem Biophys* 1974; **165**: 560–569.

45. García-Ruiz C, Morales A, Ballesta A, Rodés J, Kaplowitz N, Fernández-Checa JC. Effect of chronic ethanol feeding on glutathione and functional integrity of mitochondria in periportal and perivenous rat hepatocytes. *J Clin Invest* 1994; **94**: 193–201.
46. Han D, Ybanez MD, Johnson HS, McDonald JN, Mesropyan L, Sancheti H *et al.* Dynamic adaptation of liver mitochondria to chronic alcohol feeding in mice: biogenesis, remodeling, and functional alterations. *J Biol Chem* 2012; **287**: 42165–42179.
47. Almansa I, Fernández A, García-Ruiz C, Muriach M, Barcia JM, Miranda M *et al.* Brain mitochondrial alterations after chronic alcohol consumption. *J Physiol Biochem* 2009; **65**: 305–312.
48. Hamasaki M, Furuta N, Matsuda A, Nezu A, Yamamoto A, Fujita N *et al.* Autophagosomes form at ER-mitochondria contact sites. *Nature* 2013; **495**: 389–393.
49. Altman BJ, Rathmell JC. Metabolic stress in autophagy and cell death pathways. *Cold Spring Harb Perspect Biol* 2012; **4**: a008763.
50. Lin CW, Zhang H, Li M, Xiong X, Chen X, Chen X *et al.* Pharmacological promotion of autophagy alleviates steatosis and injury in alcoholic and non-alcoholic fatty liver conditions in mice. *J Hepatol* 2013; **58**: 993–999.
51. Lumeng L, Crabb DW. Alcoholic liver disease. *Curr Opin Gastroenterol* 2000; **16**: 208–218.
52. Yoritaka A, Hattori N, Uchida K, Tanaka M, Stadtman ER, Mizuno Y. Immunohistochemical detection of 4-hydroxynonenal protein adducts in Parkinson disease. *Proc Natl Acad Sci USA* 1996; **93**: 2696–2701.
53. Martinez-Vicente M, Talloczy Z, Wong E, Tang G, Koga H, Kaushik S *et al.* Cargo recognition failure is responsible for inefficient autophagy in Huntington's disease. *Nat Neurosci* 2010; **13**: 567–576.
54. Levine B, Yuan J. Autophagy in cell death: an innocent convict? *J Clin Invest* 2005; **115**: 2679–2688.
55. Kaarniranta K, Sinha D, Blasiak J, Kauppinen A, Veréb Z, Salminen A *et al.* Autophagy and heterophagy dysregulation leads to retinal pigmento epithelium dysfunction and development of age-related macular degeneration. *Autophagy* 2013; **9**: 973–984.
56. Viiri J, Amadio M, Marchesi N, Hyttinen JM, Kivinen N, Sironen R *et al.* Autophagy activation clears ELAVL1/HuR-mediated accumulation of SQSTM1/p62 during proteasomal inhibition in human retinal pigment epithelial cells. *PLoS One* 2013; **8**: e69563.
57. Cho DH, Nakamura T, Lipton SA. Mitochondrial dynamics in cell death and neurodegeneration. *Cell Mol Life Sci* 2010; **67**: 3435–3447.
58. Klionsky DJ, Abdalla FC, Abeliovich H, Abraham RT, Acevedo-Arozena A, Adeli K *et al.* Guidelines for the use and interpretation of assays for monitoring autophagy. *Autophagy* 2012; **8**: 445–544.
59. Ghislat G, Aguado C, Knecht E. Annexin A5 stimulates autophagy and inhibits endocytosis. *J Cell Sci* 2012; **125**: 92–107.
60. Mizushima N, Yoshimori T. How to interpret LC3 immunoblotting. *Autophagy* 2007; **3**: 542–545.

Cell Death and Disease **is an open-access journal published by** ***Nature Publishing Group*****. This work is licensed under a Creative Commons Attribution-NonCommercial-NoDerivs 3.0 Unported License. The images or other third party material in this article are included in the article's Creative Commons license, unless indicated otherwise in the credit line; if the material is not included under the Creative Commons license, users will need to obtain permission from the license holder to reproduce the material. To view a copy of this license, visit http://creativecommons.org/licenses/by-nc-nd/3.0/**